Journal of
Water & Climate Change

IWA PUBLISHING

Journal of Water and Climate Change Vol 13 No 11, 3830 doi: 10.2166/wcc.2022.215

Optimizing future mortality rate prediction of extreme temperature-related cardiovascular disease based on skewed distribution in peninsular Malaysia

Aina Izzati Mohd Esa[a], Syafrina Abdul Halim [a,*], Norhaslinda Ali[a], Jing Xiang Chung[b] and Mohd Syazwan Faisal Mohd[c]

[a] Department of Mathematics and Statistics, Faculty of Science, Universiti Putra Malaysia, UPM Serdang, Serdang 43400, Selangor, Malaysia
[b] Faculty of Science and Marine Environment, Universiti Malaysia Terengganu, Kuala Nerus 21030, Terengganu, Malaysia
[c] National Water Research Institute of Malaysia (NAHRIM), Seri Kembangan 43300, Selangor, Malaysia
*Corresponding author. E-mail: syafrina@upm.edu.my

SAH, 0000-0001-7067-9635

ABSTRACT

The bias correction method (BCM) is useful in reducing the statistically downscaled biases of global climate models' (GCM) outputs and preserving statistical moments of the hydrological series. However, BCM is less efficient under changed future conditions due to the stationary assumption and performs poorly in removing bias at extremes, thereby producing unreliable bias-corrected data. Thus, the existing BCM with normal distribution is improved by incorporating skewed distributions into the model with linear covariate (BCM-QM_{skewed}). In this study, BCM-QM_{skewed} is developed to reduce biases in the extreme temperature data of peninsular Malaysia. The input is the MIROC5 model output gridded data and observations sourced by the Malaysian Department of Irrigation and Drainage (1976–2005). BCM-QM_{skewed} with log-normal (LGNORM) and Gumbel (GUM) has shown considerable skill in correcting biases, capturing extreme and nonstationarity of current and future extreme temperatures data series corresponding to the representative concentration pathways (RCPs) for 2006–2100 based on model diagnostics and precision analysis. Higher projection of extreme temperatures is more pronounced under RCP8.5 than RCP4.5 with precise estimates ranging from 33 to 42 °C and 30 to 32 °C, respectively. Finally, the projection of extreme temperatures is used to calculate cardiovascular disease (CVD) mortality rate which coincides with high extreme temperatures ranging between 0.002 and 0.014.

Key words: bias correction, cardiovascular disease, extreme temperature, linear covariate, mortality, skewed distribution

HIGHLIGHTS

- BCM-QM_{skewed} with LGNORM and GUM was considered to capture the extreme values.
- The linear covariate model was considered to capture the nonstationary trend in extreme temperatures series.
- Results indicate the model's ability to correct the biases of extreme temperatures data for both RCPs in the study area with decent accuracy.
- Higher mortality rate of CVD is consistent with higher extreme temperatures.

1. INTRODUCTION

The impact of extreme heat events on human health is significant and diverse (Crimmins *et al.* 2016). Health is most vulnerable to extreme heat events (Patel *et al.* 2022). According to the Center for Disease Control and Prevention of United States, extreme heat events caused by high temperatures are the most prominent cause of heat-related human fatality, responsible for more deaths annually than hurricanes, fires, tornadoes, floods, and earthquakes (Vaidyanathan *et al.* 2020). Such events are expected to occur more often and are predicted to last longer because of global climate change. The World Health Organization (WHO) predicted that there will be almost 92,000 deaths annually because of heatwaves by 2030 with sub-Saharan Africa, Latin America, and southeast Asia bearing the largest burdens and extreme heat events causing more than 150,000 deaths globally from 1990 to 2018, with 2018 recorded as the warmest, particularly between June and July, through Asia, Europe, and North America, hospitalizing thousands of people with heat-related illness and recording more than 700 deaths in the immediate after-math (WHO 2019). The Intergovernmental Panel on Climate Change (IPCC) stated that

southeast Asian countries and developing countries such as Malaysia will be at the greatest risk from the emergence of extreme heat events (Stocker 2014). CVDs have been recognized as the leading cause of death throughout the world. CVDs, also known as circulatory diseases, are categorized as heart and blood vessel disorders (Patel *et al.* 2022). According to the Department of Statistics Malaysia (DOSM), coronary heart disease (CHD), one of the CVDs, was the principal cause of death in Malaysia indicating an increasing trend between 2016 and 2019 (DOSM 2017, 2018, 2019, 2020). CVD is sensitive to climate conditions; in particular, temperature-related CVDs have become a growing public health concern. Currently, the growing CVD mortality because of global warming has become a major concern, hence, an understanding of the current pattern of seasonal variations assists in estimating the impact of future climate change. Future research in the CVD mortality rate is believed to provide valuable inputs to the stakeholders for taking precautions and preventive measures to flatten the curve trend. Health-impact projection is conducted by combining estimated health-exposure relationships with projected future exposures while considering various sources of uncertainty in the analysis. Many studies found a positive correlation between the CVD mortality rate and extreme temperature. The largest number of deaths in the United States occurred because of an increase in the summer temperature (Kouis *et al.* 2019). The relationship between temperature and mortality in the 2020s and 2050s was predicted by McGeehin & Mirabelli (2001). There is a positive correlation between the temperature and CVD mortality rate (Huynen *et al.* 2001; Hajat *et al.* 2002; Kynast-Wolf *et al.* 2010; Huang *et al.* 2012). Similarly, exposure to high temperatures increases the risk of CVD mortality, particularly during summers (Moghadamnia *et al.* 2017). An increment of 1 °C in temperature is associated with a 2–5% increase in CVD mortality rate, particularly for the elderly. Paravantis *et al.* (2017) found a significant correlation of daily CVD mortality rate in people over 65 years with minimum and maximum temperatures. At a remarkably high temperature, the CVD mortality rate increased by 20–35% with a 99.9% significance level. Jackson *et al.* (2010) estimated the future number of deaths because of heat events by considering three different future scenarios. The temperature elevated risk is apparent for CVDs and respiratory causes. For instance, the estimated number of deaths under low climate scenario yielded that the greater Seattle area may expect 68, 89, and 107 excess deaths in 2025, 2045, and 2085, respectively, because of CVDs and respiratory causes among people over 45 years. Hence, there is a strong correlation between heat events and elevated risk of mortality. An estimated rise in mortality rates with an increase of 1 °C in temperature above the heat level was observed for all causes of death, including CVDs (Hajat *et al.* 2014).

Baaghideh & Mayvaneh (2017) showed a strong positive association between maximum temperature and future CVD mortality rate. An increment of 1 °C is associated with a 4.27% increase in the CVD mortality rate in the following decades. Li *et al.* (2018) studied the projections of the burden of CVDs attributable to future temperatures. Future changes in climate are likely to cause an increment in heat-related CVDs. The monthly analysis showed that the most significant increase will occur in the summer, with percentage changes greater than 150% in the 2050s and up to 300% in the 2070s. Huang *et al.* (2019) further projected the relationship between future temperature and CHD mortality in the elderly. The annual temperature-related CHD mortality in the 2050s and 2070s was greater than the baseline. Liu *et al.* (2019) projected heat-related mortality for all causes of death including CVDs in the 2030s, 2060s, and 2090s relative to the baseline period. The projected heat-related mortality would cause a substantial increase in the majority of the GCMs with population growth, adaptation, and ageing. Gu *et al.* (2020) projected temperature-related mortality of CVDs under different climate scenarios with that of CHD burden showing an increase from 4.40 to 6.02% primarily because of people having heat-sensitive diseases.

Projection of climate change impact including health impact is often studied using the GCM (Noor *et al.* 2018). However, the GCM outputs cannot provide reliable information on spatial scales below 200 km, and therefore, cannot be used for local impact studies (Amirabadizadeh *et al.* 2016; Noor *et al.* 2018; Adeyeri *et al.* 2020). Additionally, there are several errors and uncertainties in GCM outputs (Amirabadizadeh *et al.* 2016; Noor *et al.* 2018; Adeyeri *et al.* 2020). To assess climate change on local scales, an approach known as downscaling is used to bridge the gap between the resolution of GCM outputs and the local climatic process (Noor *et al.* 2018). Murphy (1999) concluded that both dynamical and statistical downscaling exhibit similar skill levels and produce hydrologically plausible results with the former being more sensitive to climate change with respect to future climate scenarios. However, these two approaches can nonetheless differ significantly in their projections of future climate conditions. Murphy (1999) and Wilby *et al.* (2000) also highlighted the need to bias correct GCM outputs to assure meaningful results in meteorological applications. This has been supported by Shrestha *et al.* (2014) who stated that there is good agreement between statistically downscaled GCM simulated temperature with the observations, whereas the dynamically downscaled simulated results differ substantially from observations. However, the differences between the 2050s and 1970s obtained from the two approaches are qualitatively similar. Shaaban *et al.* (2011) concluded that dynamical

downscaling can produce more reliable results than statistical downscaling as it does not incorporate the time evolution of dynamical features on the climate at continental and global scales. However, Wilby *et al.* (2000) argued that statistical downscaling has shown good performance to reduce biases for temperature and it has the advantage of efficiently producing ensembles of surface climate variables given by a limited set of gridded predictor variables. In contrast, producing dynamically downscaled outputs was the most time consuming and computationally demanding. Despite the higher level of sophistication and physical realism of the model, dynamical downscaling was not generally as efficient as statistical downscaling and does not depend on static regression relationships among physical processes. Overall, statistically downscaled GCM outputs remain the preferred approach provided that biases are explicitly accounted for. To date, there are no truly objective techniques for identifying which particular downscaling approach is the best or most competent in generating future climate projections for a given region and climate variables (Conlon *et al.* 2016; Smid & Costa 2018; Bettolli *et al.* 2021; Wang *et al.* 2022). Various aspects of the atmospheric system, which each model handles differently, may be altered as the climate changes. Conlon *et al.* (2016) and Jose *et al.* (2022) suggested that to assess the best climate projection, an ensemble mean value of GCMs projection needs to be produced. In addition to considering the mean change across a set of models, it is useful to identify the most and least extreme projections within a suite of climate-model outputs. Smid & Costa (2018) suggested that the most cutting-edge approach to provide future localized climate information is to combine dynamical downscaling with further statistical downscaling when assessing the climate evolution. However, the skills, expertise, access to funding and time computational power resources were arguably outstanding.

Future climate change exposures are typically derived using simulations from computationally expensive climate models. Even though these models reflect state-of-the-art knowledge on the climate system, their outputs are known to exhibit complex spatial–temporal biases when compared to observations. Factors contributing to this bias include errors in parameters describing physical and chemical processes, incorrect representation of the underlying processes with mathematical equations, and discretization of meteorological fields in space and in time. Hence, climate-model simulations for the projection period need to be bias-corrected prior to estimating future health impacts (Holthuijzen *et al.* 2021). BCM is renowned in statistical downscaling because it can reduce biases between GCM outputs and observations, and it skillfully reduces the coarse resolution of GCMs outputs into a finer resolution of observation scale (Teutschbein & Seibert 2012; Cannon *et al.* 2015; Fang *et al.* 2015; Ringard *et al.* 2017; Hong *et al.* 2022; Ngai *et al.* 2022). Wood *et al.* (2004) employed BCM to reduce the statistically downscaled biases of GCM outputs. BCM was successful in reproducing the main features of the observed hydrometeorology from the retrospective climate simulation, when applied to statistically downscaled GCM outputs, and competent to preserve the statistical moments of the hydrological series (Sennikovs & Bethers 2009). Generally, BCM for future simulation is accomplished in two steps. First, the bias between observations and simulations during the historical/estimated period is assessed. Then a correction algorithm is applied to future simulations by assuming the bias can be extrapolated to future periods. Olsson *et al.* (2015) stated that quantile mapping was able to provide temperature data that were sufficiently close to observed discharges in the control period and produced more realistic projections for mean annual and seasonal changes compared to the uncorrected GCM data. Putra *et al.* (2020) have found that BCM could reduce biases in the GCM outputs relative to observations with a coefficient of determination of 0.81 for spatial distribution. Tadese *et al.* (2020) also showed that BCM and variance scaling performed well in correcting the biases in GCM outputs despite the corrected maximum and minimum temperature being slightly overestimated for the mean and standard deviation. Despite the fact that BCM has shown considerable skill in reducing the biases, there are a few limitations that need to be addressed. Firstly, the remaining uncertainty regarding how well a calibrated BCM performs for conditions different from those used for calibration. Although a good performance of BCM during the calibration period has been shown, that does not guarantee a good performance under changed future conditions due to the stationary assumption of BCM. Secondly, BCM is less efficient in downscaling both high and low temperature extremes (Maurer & Hidalgo 2008; Abatzoglou & Brown 2012). The most commonly used BCMs were based on shifting or scaling climate-model simulations that have been shown to perform poorly for removing bias at extremes (Räisänen & Räty 2013). Thus, BCM has a tendency to overfit on calibration data, especially at extremes where data are scarce and highly variable (Piani *et al.* 2010; Grillakis *et al.* 2013; Lafon *et al.* 2013; Mamalakis *et al.* 2017; Holthuijzen *et al.* 2021). The limitation of BCM is mainly because it assumes that the temperature follows the normal distribution (Hempel *et al.* 2013; Gaitán *et al.* 2019; Lange 2019). Some studies recommended the normal to be the most appropriate distribution for describing the statistical properties of extreme temperatures (Zhan *et al.* 2020). However, Semenov (2008) concluded that normal is not a good fit. The means of yearly maxima for daily maximum temperature were reproduced less accurately compared to those outside the 95% confidence interval (CI) of observed means. The study suggested replacing the normal distribution with a more flexible distribution.

Similarly, Barrow & Hulme (1996) proposed that normal distribution could yield accurate results when variations in the temperature were less than 0.1 °C, but produced errors for variations greater than 10 °C. BCM with gamma (GAM) distribution further decreased the simulation biases. Similarly, Pastén-Zapata *et al.* (2020) tested BCM in simulating the temperature and observed that the existing BCM with normal distribution did not improve the representation of daily temporal variability, especially the extremes. These findings are significant for tackling the main part of the statistical modeling process which is the selection of appropriate distribution for the BCM that could be overlooked in the past research. Various studies were conducted to fit a suitable statistical distribution on extreme temperatures and different conclusions were drawn depending on factors such as the area and duration of study. Particularly, the right distribution may enhance the BCM's performance in simulating the extremes. Several studies suggested GAM and GUM owing to their capability to capture the mean and variance of daily extreme temperatures (Folland *et al.* 1999; Jones *et al.* 1999; Horton *et al.* 2001). Other studies concluded that Weibull (WEI) is a good fit for both maximum and minimum temperature data (Seimela 2021), whereas several studies fitted daily extreme temperatures with generalized extreme value (GEV) distribution (Kharin & Zwiers 2005; Underwood 2013; An *et al.* 2020). Wilson (2016) revealed that the GEV distribution was better in modeling the extreme temperature behavior based on the lowest values of the Akaike information criterion (AIC) and Bayesian information criterion (BIC). Two comparative tests, namely, Anderson–Darling and Kolmogorov–Smirnov, confirmed that the GEV distribution is adequate for the data. Similarly, in Malaysia, Amin *et al.* (2018) concluded that Frèchet (FRE) and GEV are a better fit for monthly maximum temperature. GEV was observed to be suitable for a daily and annual maximum of daily maximum temperature data (Salleh & Hasan 2018). Results indicated that the nonstationary model is preferable for Kuala Terengganu, Muadzam Shah, and Senai stations. Hasan *et al.* (2013) and Hasan *et al.* (2014) fitted the annual extreme temperatures in Malaysia with the GEV distribution. Additionally, nonstationary GEV has been observed to perform better than the stationary GEV for several stations such as Subang, Bayan Lepas, Kota Kinabalu, Sibu, and Labuan. Hasan *et al.* (2014) applied cluster analysis on the studied stations, thereby revealing similarities that indicate the best performance of the nonstationary GEV distribution. Contrarily, Supian & Hasan (2021) compared several distributions to find the best distribution for fitting the annual extreme temperatures. The results indicated that a majority of stations preferred the generalized skew logistic distribution as the best fitted probability distribution. Some studies indicated excellent performances of the normal, LGNORM, and WEI distributions to describe the annual extreme temperature. In summary, no single distribution can be concluded to perform the best. Therefore, it is crucial to thoroughly analyze various aspects while selecting the most appropriate distribution for the extreme temperatures to achieve an accurate projection of the CVD mortality rate. Thus, in this study, the two issues in BCM will be solved by incorporating the skewed distribution to fit the extreme values of annual temperatures and to include the linear covariate to take into account nonstationarity (i.e., linear trend) in the data series. Hence, the main objectives are to identify a better statistical distribution among the skewed distributions (i.e., LGNORM, GAM, Pearson type 3 (P3), GEV, GUM, WEI, and FRE distributions), formulate the BCM-QM_{skewed} with better statistical distribution and linear covariate in reducing the biases between the historical/estimated and observed annual extreme temperatures in peninsular Malaysia and project the mortality rate of CVD based on annual extreme temperatures projection in peninsular Malaysia using the annual attributable death (AAD) equation.

2. METHODS

2.1. Study area

Malaysia is located in southeast Asia and consists of the following two regions: peninsular Malaysia and east Malaysia. Owing to its geographical location, it experiences two monsoons, the northeast and southwest monsoons; the former occurs between November and January with an average temperature between 29 and 30 °C (i.e., wet season) and the latter occurs between March and August with an average temperature of 32–33 °C (i.e., dry season). Suparta & Yatim (2017) stated that the lowest and highest heatwave indexes across east Malaysia from 2008 to 2010 occurred in Kuching and Sandakan with 27.3 and 35.0 °C, respectively. From 2001 to 2010 across peninsular Malaysia, the highest heatwave index was recorded in Kuala Lumpur with an increment of 9.1 °C and the lowest heatwave was recorded in Alor Setar with an increment of 0.1 °C. A moderate heatwave index was observed in Kuantan with 4.2 °C and the longest heatwave of 24 days occurred in Ipoh, Perak, with amplitude between 29.4 and 33.0 °C. The characteristics of the heatwave were compared to the spatial distribution maps showing that southeast, northeast, and western part of Malaysia experience more heatwave. The maximum heatwave index was more pronounced between March and July during the dry season (Suparta & Yatim 2019), indicating that the extreme heat events in Malaysia are a growing problem. Hence, owing to the significant and direct impact of heat

events on various sectors including human health, critical study and exploration are required (Suparta & Yatim 2017, 2019). This study focuses on peninsular Malaysia where most of the urban and developing cities more vulnerable to heat exposure are located. Figure 1 shows the locations of stations throughout peninsular Malaysia.

2.2. Dataset

In this study, observed extreme temperatures (1976–2005), historical/estimated extreme temperatures (1976–2005), future extreme temperatures (2006–2100), and observed mortality (1990–2017) data recorded annually were used. The secondary data of observed daily temperature data series between 1976 and 2005 in peninsular Malaysia were obtained from the Malaysian Department of Irrigation and Drainage (Wong *et al.* 2011). Then, the annual extreme temperatures were extracted using the block maxima approach. Similarly, the historical/estimated (1976–2005) and future (2006–2100) GCMs of annual extreme temperatures were obtained under moderate and worst-case future scenarios of RCPs known as RCP4.5 (moderate case) and RCP8.5 (worst case). The model for interdisciplinary research on climate (MIROC5) under the Coupled Model Intercomparison Project 5 (CMIP5) with resolution 1.406° × 1.4° (Williams *et al.* 2012) was used. The definitions of both RCPs are presented in Appendix 1. The secondary data of annually observed mortality rate of CVD between 1990 and 2017 in peninsular Malaysia were obtained from the Global Burden of Disease Collaborative Network (http://ghdx.healthdata.org/gbd-results-tool) (Roth 2018). This database is openly available and can be downloaded from the global health data exchange web portal.

2.3. Statistical procedure

The transfer function of the BCM-QM$_{skewed}$ technique is defined as (Enayati *et al.* 2021),

$$x_{corr} = \mathrm{CDF}(x_o)^{-1}[\mathrm{CDF}(x_m)] \quad (1)$$

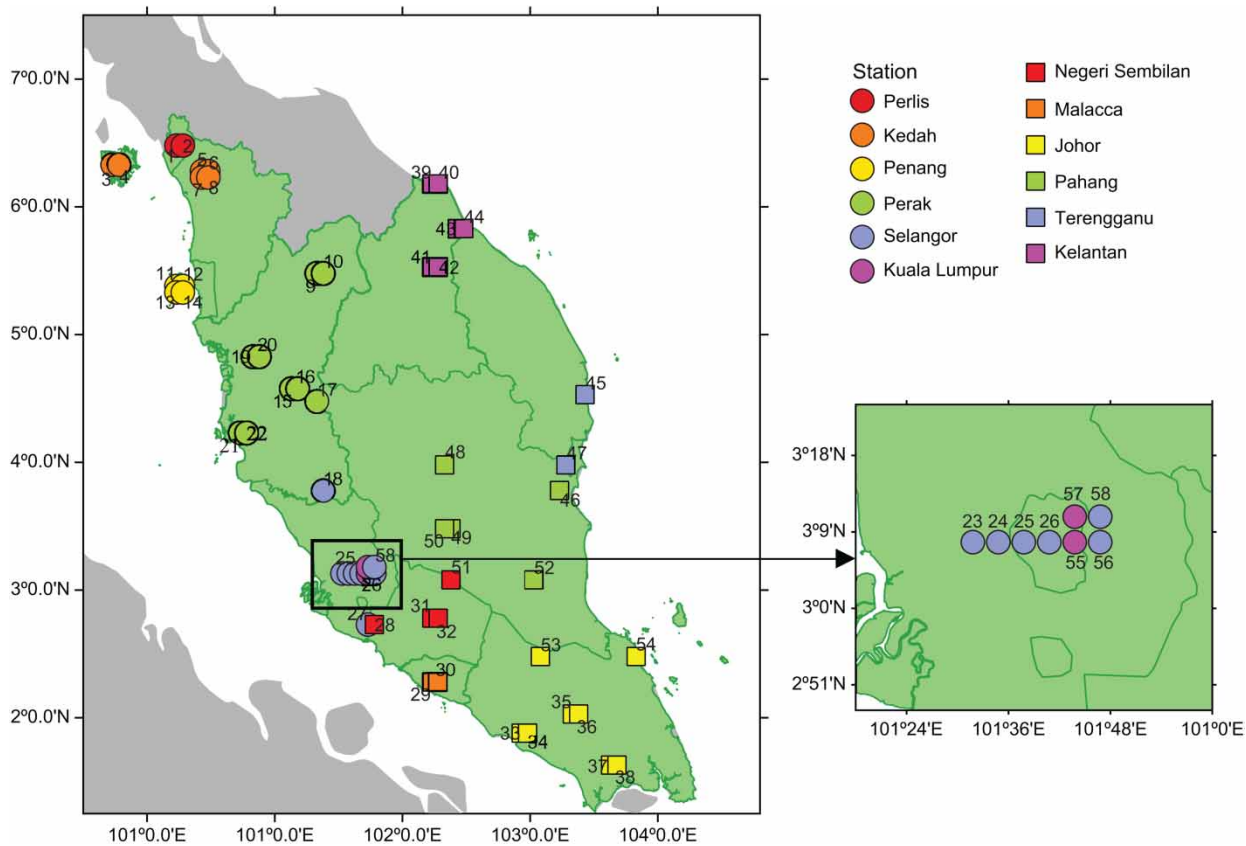

Figure 1 | Location of stations throughout peninsular Malaysia.

where x_{corr} is the corrected temperature between observed and historical/estimated model output gridded GCM annual extreme temperatures; x_o is the annual extreme temperatures of observations; x_m is the annual extreme temperatures of historical/estimated model output gridded GCM. The cumulative distribution function of LGNORM, GAM, P3, GEV, GUM, WEI, and FRE distributions are considered in Equation (1). To handle nonstationarity, a linear (i.e., time-varying) covariate is proposed. All parameters are estimated using the maximum likelihood estimation method. The models are outlined below, where μ, σ, α refer to the location, scale, and shape parameters, respectively. t refers to the unit of the selection period (annually) with $t = 1976, \ldots, 2005$ while σ is in the form of an exponential function to ensure that the estimated parameters are always positive (Coles *et al.* 2001; Ng *et al.* 2022).

Model 1 (M1): μ, σ and α are constants (i.e., stationary model)

Model 2 (M2): $\mu(t) = \mu_0 + \mu_1 t$, σ and α are constants (i.e., nonstationary model)

Model 3 (M3): $\sigma(t) = \exp(\sigma_0 + \sigma_1 t)$, μ and α are constants (i.e., nonstationary model)

Model 4 (M4): $\mu(t) = \mu_0 + \mu_1 t$ & $\sigma(t) = \exp(\sigma_0 + \sigma_1 t)$, α is constant (i.e., nonstationary model)

The log-likelihood function for M2, M3, and M4 of LGNORM is,

$$\ln L = -n\ln\sigma - \sum_{i=1}^{n}\ln x_i - \frac{n}{2}\ln 2\pi - \sum_{i=1}^{n}\frac{(\ln x_i - (\mu_0 + \mu_1 t_i))^2}{2\sigma^2}$$

$$\ln L = -n\ln\sigma - \sum_{i=1}^{n}\ln x_i - \frac{n}{2}\ln 2\pi - \sum_{i=1}^{n}\frac{(\ln x_i - (\mu_0 + \mu_1 t_i))^2}{2(\exp^{(\sigma_0+\sigma_1 t_i)})^2}$$

$$\ln L = -n\ln\sigma - \sum_{i=1}^{n}\ln x_i - \frac{n}{2}\ln 2\pi - \sum_{i=1}^{n}\frac{((\ln x_i - (\mu_0 + \mu_1 t_i))^2)}{2(\exp^{(\sigma_0+\sigma_1 t_i)})^2} \quad (2)$$

where $\mu(t) = \mu_0 + \mu_1 t$ and $\sigma(t) = \exp^{(\sigma_0+\sigma_1 t)}$.

The log-likelihood function for M3 of GAM is,

$$\ln L = (\alpha - 1)\sum_{i=1}^{n}\ln\left(\frac{x_i}{\exp^{(\sigma_0+\sigma_1 t_i)}}\right) + \sum_{i=1}^{n}\left(\frac{-x_i}{\exp^{(\sigma_0+\sigma_1 t_i)}}\right) - n\sum_{i=1}^{n}(\sigma_0 + \sigma_1 t_i) - n\ln\gamma(\alpha) \quad (3)$$

where $\sigma(t) = \exp^{(\sigma_0+\sigma_1 t)}$.

The log-likelihood function for M2, M3, and M4 of P3 is,

$$\ln L = (\alpha - 1)\sum_{i=1}^{n}\ln\left(\frac{x_i - (\mu_0 + \mu_1 t_i)}{\sigma}\right) + \sum_{i=1}^{n}\left(\frac{x_i - (\mu_0 + \mu_1 t_i)}{\sigma}\right) - n\ln\sigma - n\ln\gamma(\alpha)$$

$$\ln L = (\alpha - 1)\sum_{i=1}^{n}\ln\left(\frac{x_i - \mu}{\exp^{(\sigma_0+\sigma_1 t_i)}}\right) + \sum_{i=1}^{n}\left(\frac{x_i - \mu}{\exp^{(\sigma_0+\sigma_1 t_i)}}\right) - n\sum_{i=1}^{n}(\sigma_0 + \sigma_1 t_i) - n\ln\gamma(\alpha)$$

$$\ln L = (\alpha - 1)\sum_{i=1}^{n}\ln\left(\frac{x_i - (\mu_0 + \mu_1 t_i)}{\exp^{(\sigma_0+\sigma_1 t_i)}}\right) + \sum_{i=1}^{n}\left(\frac{x_i - (\mu_0 + \mu_1 t_i)}{\exp^{(\sigma_0+\sigma_1 t_i)}}\right) - n\sum_{i=1}^{n}(\sigma_0 + \sigma_1 t_i) - n\ln\gamma(\alpha) \quad (4)$$

where $\mu(t) = \mu_0 + \mu_1 t$ and $\sigma(t) = \exp^{(\sigma_0+\sigma_1 t)}$.

The log-likelihood function for M2, M3, and M4 of GEV is,

$$\ln L = -n\ln\sigma + \sum_{i=1}^{n}\left[\left(\frac{1}{\alpha}-1\right)\ln\left(1-\frac{\alpha(x_i-(\mu_0+\mu_1 t_i))}{\sigma}\right)-\left(\frac{\alpha(x_i-(\mu_0+\mu_1 t_i))}{\sigma}\right)^{\frac{1}{\alpha}}\right]$$

$$\ln L = -n\sum_{i=1}^{n}(\sigma_0+\sigma_1 t_i) + \sum_{i=1}^{n}\left[\left(\frac{1}{\alpha}-1\right)\ln\left(1-\frac{\alpha(x_i-\mu)}{\exp^{(\sigma_0+\sigma_1 t_i)}}\right)-\left(\frac{\alpha(x_i-\mu)}{\exp^{(\sigma_0+\sigma_1 t_i)}}\right)^{\frac{1}{\alpha}}\right]$$

$$\ln L = -n\sum_{i=1}^{n}(\sigma_0+\sigma_1 t_i) + \sum_{i=1}^{n}\left[\left(\frac{1}{\alpha}-1\right)\ln\left(1-\frac{\alpha(x_i-(\mu_0+\mu_1 t_i))}{\exp^{(\sigma_0+\sigma_1 t_i)}}\right)-\left(\frac{\alpha(x_i-(\mu_0+\mu_1 t_i))}{\exp^{(\sigma_0+\sigma_1 t_i)}}\right)^{\frac{1}{\alpha}}\right] \quad (5)$$

where $\mu(t) = \mu_0 + \mu_1 t$ and $\sigma(t) = \exp^{(\sigma_0+\sigma_1 t)}$.

The log-likelihood function for M2, M3, and M4 of GUM is,

$$\ln L = -\sum_{i=1}^{n}\left(\frac{x_i-(\mu_0+\mu_1 t_i)}{\sigma}\right) - \ln\sigma - \sum_{i=1}^{n}\exp\left(-\frac{(x_i-(\mu_0+\mu_1 t_i))}{\sigma}\right)$$

$$\ln L = -\sum_{i=1}^{n}\left(\frac{x_i-\mu}{\exp^{(\sigma_0+\sigma_1 t_i)}}\right) - n\sum_{i=1}^{n}(\sigma_0+\sigma_1 t_i) - \sum_{i=1}^{n}\exp\left(-\frac{(x_i-\mu)}{\exp^{(\sigma_0+\sigma_1 t_i)}}\right)$$

$$\ln L = -\sum_{i=1}^{n}\left(\frac{x_i-(\mu_0+\mu_1 t_i)}{\exp^{(\sigma_0+\sigma_1 t_i)}}\right) - n\sum_{i=1}^{n}(\sigma_0+\sigma_1 t_i) - \sum_{i=1}^{n}\exp\left(-\frac{(x_i-(\mu_0+\mu_1 t_i))}{\exp^{(\sigma_0+\sigma_1 t_i)}}\right) \quad (6)$$

where $\mu(t) = \mu_0 + \mu_1 t$ and $\sigma(t) = exp^{(\sigma_0+\sigma_1 t)}$.

The log-likelihood function for M3 of WEI is,

$$\ln L = n\ln\alpha - n\alpha\sum_{i=1}^{n}(\sigma_0+\sigma_1 t_i) + (\alpha-1)\sum_{i=1}^{n}\ln x_i - \sum_{i=1}^{n}\left(\frac{x_i}{\exp^{(\sigma_0+\sigma_1 t_i)}}\right)^{\alpha} \quad (7)$$

where $\sigma(t) = \exp^{(\sigma_0+\sigma_1 t)}$.

The log-likelihood function for M3 of FRE is,

$$\ln L = n(\sigma_0+\sigma_1 t) + n\ln\alpha - (\alpha+1)\sum_{i=1}^{n}\ln x_i - (\exp^{(\sigma_0+\sigma_1 t_i)})\sum_{i=1}^{n}x_i^{-\alpha} \quad (8)$$

where $\sigma(t) = \exp^{(\sigma_0+\sigma_1 t)}$.

The projection period of future temperature series in the 21st century is divided into the following three periods: early (2006–2035), mid- (2036–2065), and late (2066–2100) (Tangang *et al.* 2020). $x_{RCP4.5}$ represents the values of future annual extreme temperatures under RCP4.5, and $x_{RCP8.5}$ represents the values of future annual extreme temperatures under RCP8.5. Accordingly, the transfer functions of the BCM-QM$_{skewed}$ technique for future annual extreme temperatures under RCP4.5 and RCP8.5 are,

$$\begin{aligned} x_{RCP4.5(corr)} &= \mathrm{CDF}(x_{corr})^{-1}[\mathrm{CDF}(x_{RCP4.5})] \\ x_{RCP8.5(corr)} &= \mathrm{CDF}(x_{corr})^{-1}[\mathrm{CDF}(x_{RCP8.5})] \end{aligned} \quad (9)$$

where $x_{RCP4.5}$ is the raw future annual extreme maximum temperature under RCP4.5, $x_{RCP8.5}$ is the raw future annual extreme maximum temperature under RCP8.5, $x_{RCP4.5(corr)}$ is the projection of future annual maximum temperature under RCP4.5, and $x_{RCP8.5(corr)}$ is the projection of future annual maximum temperature under RCP8.5. The AAD equation is used to project the impact of temperature on CVD mortality rates in the future (2006–2100) (Li *et al.* 2013),

$$\mathrm{AAD} = y_0 \times \mathrm{ERC} \tag{10}$$

where y_0 represents the baseline annual mortality, and ERC represents the attributable change in CVD mortality at each temperature. A distributed lag nonlinear model is used to model the relationship between temperature and CVD mortality (Gasparrini 2013), which has the advantage of capturing the lagged dependencies of exposure–response relationships by using two-function modeling which are the lag–response and exposure–response relationships. These relationships are then incorporated into the cross-basis function that accounts for a lag of 21 days. In the exposure–response relationship, a quadratic B-spline is used, while in the lag–response relationship, a natural cubic B-spline is used (De' Donato *et al.* 2015; Vicedo-Cabrera *et al.* 2019). The relationship between temperature and CVD mortality can be observed using the relative risk (RR) value that is distributed differently across time (Vicedo-Cabrera *et al.* 2019).

The AIC and the BIC provide measures of model performance that account for model complexity. AIC and BIC combine a term reflecting how well the model fits the data with a term that penalizes the model in proportion to its number of parameters. The AIC is an estimator for prediction error, and an indicator of the relative quality of statistical models for a given set of data. The equation for AIC is (Coles *et al.* 2001),

$$\mathrm{AIC} = 2k - 2(\ln L) \tag{11}$$

where k is the number of parameters, and $\ln L$ is the negative log-likelihood function. The BIC is a criterion for model selection among a finite set of models, such that the models with lower BIC are generally preferred. The equation for BIC is (Coles *et al.* 2001),

$$\mathrm{BIC} = k(\ln(n)) - 2(\ln L) \tag{12}$$

where n is the sample size, k is the number of parameters, and $\ln L$ is the negative log-likelihood function. The likelihood-ratio test (LRT) is a hypothesis test that chooses the best model between two nested models based on the ratio of their likelihoods, specifically, by maximizing over the entire parameter space after imposing some constraint. The deviance statistic, D of LRT is (Coles *et al.* 2001),

$$D = -2(\ln L_s - \ln L_n) \tag{13}$$

where $\ln L_s$ is the negative log-likelihood function for a simple model (i.e., constant or stationary M1), and $\ln L_n$ is the negative log-likelihood function for a nested model with covariates or nonstationary M2, M3, and M4. The precision analysis is performed to validate the results of corrected and future extreme temperatures, and current and future CVD mortality rates. The performance of BCM-QM_{skewed} can be evaluated using the root mean square error (RMSE), mean absolute error (MAE), percent bias (PBIAS), and predictive precision (PP) as in Equation (14) (Etemadi *et al.* 2014; Sridhar *et al.* 2016), where x_o is the observed annual extreme temperatures, and x_{corr} is the corrected annual

extreme temperatures.

$$\text{RMSE} = \sqrt{\frac{\sum_{i=1}^{n} (x_o i - x_{\text{corr}} i)^2}{n}}$$

$$\text{MAE} = \frac{\sum_{i=1}^{n} |x_o i - x_{\text{corr}} i|}{n}$$

$$\text{PBIAS} = \frac{\sum_{i=1}^{n} (x_o i - x_{\text{corr}} i) * 100}{\sum_{i=1}^{n} x_o i} \tag{14}$$

$$\%\text{PE} = \sum_{i=1}^{n} \left(\frac{x_{o_i} - x_{\text{corr}_i}}{x_{o_i}} \right) * 100$$

$$\sqrt{\sum_{i=1}^{n} \frac{(\%PE_i - \overline{PE})}{n}} \quad \text{for } i = 1, \ldots, n = 30$$

3. RESULTS AND DISCUSSION

3.1. Statistical distribution of extreme temperatures

Understanding and accounting for nonstationary patterns in meteorological/hydrological data are among the greatest challenges requiring accurate future projections to properly plan risk mitigation. The problem of nonstationarity occurs because of industrialization and urbanization that could influence the change in climatic conditions, which causes the meteorological data to become nonstationary (Raggad 2018). Misleading application of nonstationarity would cause unexpected loss, underestimation of variability, and other uncertain events. Therefore, numerous studies on nonstationarity are being conducted to predict/project future events under fluctuating environmental conditions. Various studies focus on the nonstationary frequency analysis that initially takes several covariates into account, such as time to capture the trend revealed in the series (i.e., linear, seasonal). In this study, a time-varying covariate was considered for modeling, dealing with nonstationarity in the data series, and capturing the positive linear trend in the series of datasets. Particularly, both constant and time-varying covariate models of LGNORM, GAM, P3, GEV, GUM, WEI, and FRE distributions were fitted to the annual extreme temperatures. The well-fitted distribution was selected based on the lowest values of AIC and BIC. The nonstationary models with time-varying covariate were suitable for stations 9–38, 41–42, and 45–58, as shown in Table 1. In general, it can be concluded that LGNORM and GUM are the most suitable distributions to model the annual extreme temperatures at stations throughout peninsular Malaysia. LGNORM and GUM are the most suitable models to fit the annual extreme temperatures for stations in the western and eastern parts, respectively. It can also be inferred that a nonstationary model with a time-varying covariate is a well-fitted model for annual extreme temperatures at most stations across peninsular Malaysia, suggesting that the trend of extreme temperatures increased between 1976 and 2005. To verify these findings, LRT was performed on the nested model, whereas nonnested models were not tested (e.g., stations 5–10, 21–32, 37–38, and 55–58). The significance of adding the time-varying covariate into the model was tested at a significance level of 0.05. Stations 1–4, 39–40, and 43–44 have p-values greater than 0.05, leading to the acceptance of H_0, thus proving that the stationary model is suitable for all these stations (Appendix 2). However, the remaining stations verified that the nonstationary model is well fitted. These results are consistent with the AIC and BIC values. The estimated parameter values fall within the range of CI with 95% confidence (see Appendix 3). Furthermore, smaller standard error (SE) values could also indicate more precise estimates of a population parameter. The 95% CI produces ranges usually within the population parameter, thereby providing meaningful estimates. The width of CI indicates the precision of an estimate, and the margin of error indicates the uncertainty associated with estimating an entire population from a sample. If the range is narrow, the estimate is precise because the margin of error is small, with only a small range of plausible values (Higgins *et al.* 2019). Therefore, larger intervals lead to larger values of margin of error, and the parameter is likely to fall within that wider range, resulting in an imprecise estimate. The 95% CI

Table 1 | Suitable distribution for all stations with corresponding AIC and BIC values

	Distribution		Constant		Time-varying covariate	
Station	Constant	Time-varying covariate	AIC	BIC	AIC	BIC
1	**LGNORM**	LGNORM (M2)	37.29	40.09	38.19	42.39
2	**LGNORM**	LGNORM (M2)	36.13	38.94	37.15	41.35
3	**LGNORM**	LGNORM (M1)	34.45	37.25	35.36	39.57
4	**LGNORM**	LGNORM (M1)	34.36	37.16	34.85	39.05
5	**GUM**	LGNORM	33.24	36.04	34.12	38.32
6	**GUM**	LGNORM	32.2	35	33.17	37.38
7	**GUM**	LGNORM	33.1	35.9	33.81	38.01
8	**GUM**	LGNORM	31.54	34.34	32.46	36.66
9	LGNORM	**GUM (M1)**	27.91	30.72	22.45	26.65
10	LGNORM	**GUM (M1)**	28.03	30.83	22.74	26.94
11	GUM	**GUM (M1)**	28.79	31.6	20.04	24.24
12	GUM	**GUM (M1)**	28.76	31.56	19.02	23.22
13	GUM	**GUM (M1)**	29.63	32.43	19.37	23.58
14	GUM	**GUM (M1)**	29.55	32.35	18.69	22.89
15	NORM	**LGNORM**	46.22	49.03	24.02	28.23
16	NORM	**LGNORM**	49.79	52.59	23.62	27.82
17	NORM	**LGNORM**	51.63	54.44	22.34	26.54
18	NORM	**LGNORM**	58.46	61.27	24.75	28.95
19	LGNORM	**LGNORM**	43.49	46.29	23.8	28
20	LGNORM	**LGNORM**	42.86	45.67	23.89	28.09
21	NORM	**GUM (M4)**	41.54	44.34	19.68	25.28
22	NORM	**GUM (M4)**	42.63	45.44	19.94	25.54
23	GUM	**GUM (M1)**	68.49	71.29	30.44	34.65
24	GUM	**GUM (M1)**	70.26	73.07	30.97	35.17
25	GUM	**GUM (M1)**	69.91	72.72	31.58	35.79
26	GUM	**GUM (M1)**	68.05	70.86	31.41	35.61
27	GUM	**GUM (M1)**	66.23	69.04	35.33	39.53
28	GUM	**GUM (M1)**	66.01	68.81	35.59	39.79
29	GUM	**GUM (M1)**	59.16	61.96	37.36	41.56
30	GUM	**GUM (M1)**	57.96	60.76	41.35	45.55
31	GUM	**GUM (M1)**	63.63	66.43	40.76	44.96
32	GUM	**GUM (M1)**	63.62	66.43	41.91	46.11
33	LGNORM	**LGNORM**	52.78	55.58	37.77	41.97
34	LGNORM	**LGNORM**	52.31	55.11	37.51	41.71
35	LGNORM	**LGNORM**	49.54	52.34	37.04	41.25
36	LGNORM	**LGNORM**	49.09	51.89	36.37	40.57
37	LGNORM	**GUM (M1)**	45.98	48.78	33.82	38.02
38	LGNORM	**GUM (M1)**	44.52	47.32	31.13	35.34
39	**GUM**	GUM (M1)	23.08	25.88	23.75	27.95
40	**GUM**	GUM (M1)	24.24	27.04	24.55	28.76
41	GUM	**GUM (M1)**	32.03	34.83	28.8	33.01

(*Continued.*)

Table 1 | Continued

	Distribution		Constant		Time-varying covariate	
Station	Constant	Time-varying covariate	AIC	BIC	AIC	BIC
42	GUM	**GUM (M1)**	32.42	35.22	29.07	33.28
43	**GUM**	GUM (M1)	27.31	30.11	26.4	30.61
44	**GUM**	GUM (M1)	24.17	26.97	23.88	28.08
45	GUM	**GUM (M1)**	64.14	66.94	60.5	64.71
46	GUM	**GUM (M1)**	71.99	74.79	68.9	73.1
47	GUM	**GUM (M1)**	71.23	74.03	67.76	71.96
48	LGNORM	**LGNORM**	63.18	65.98	47.82	52.02
49	LGNORM	**LGNORM**	63.74	66.54	44.95	49.15
50	LGNORM	**LGNORM**	63.81	66.61	42.57	46.77
51	LGNORM	**LGNORM**	64.04	66.85	41.58	45.78
52	GUM	**LGNORM**	66.26	69.06	60.19	64.4
53	GUM	**GUM (M4)**	55.26	58.07	37.53	43.13
54	GUM	**GUM (M4)**	48.72	51.52	41.01	46.62
55	GUM	**GUM (M1)**	67.36	70.17	31.7	35.9
56	GUM	**GUM (M1)**	67.16	69.96	32.16	36.37
57	GUM	**GUM (M1)**	67.56	70.36	31.61	35.81
58	GUM	**GUM (M1)**	67.06	69.86	31.85	36.05

Bold fonts refer to good model.

indicates a small width interval and margin of error for each parameter, verifying that the estimated parameter values are good estimates for all stations. Generally, the distributions of all stations are positively skewed and only a few stations exhibit fairly symmetrical distribution. Figure 2 shows an example of quantile and density plots of annual extreme temperatures for station 42. The closer the point to the straight line, the better the model in which all stations satisfy the criteria.

3.2. Precision analysis of BCM-QM$_{skewed}$ and projection of future extreme temperatures

Subsequently, precision analysis was conducted on the fitted model to assess the performance of BCM-QM$_{skewed}$ in handling the source of bias in the GCM model. The RMSE and MAE of the observations (see Appendix 4) were calculated as a function of the corrected annual extreme temperatures, which vary from the optimal value of 0 to a large positive value with smaller values indicating good model simulation. The lowest RMSE and MAE values show a strong relationship, indicating better simulation (Etemadi *et al.* 2014) and good BCM-QM$_{skewed}$ performance. According to Etemadi *et al.* (2014), the optimal value of PBIAS is 0, indicating an accurate model simulation, whereas positive and negative values indicate model underestimation and overestimation bias, respectively. Furthermore, PP was calculated to verify the results, as it shows the change in the standard deviation of the proposed model (Sridhar *et al.* 2016). Hence, the BCM-QM$_{skewed}$ technique performed well in reducing the bias from the GCM model for all stations, i.e., the corrected annual extreme temperatures are comparable to the observed values. Figure 3 shows the boxplot and density plots of the extreme temperatures' series for station 42 demonstrating that the BCM-QM$_{skewed}$ technique is able to correct the bias successfully. There are several stations that produced one or two outliers of corrected annual extreme temperatures based on the boxplot in which most annual extreme temperatures are skewed to the right (long right tails) (Suhaila & Yusop 2018). Figure 4 shows the trend in extreme temperatures, which is projected to increase for both RCPs at station 42. However, the long positive skewness is more pronounced for the projection under RCP8.5 than RCP4.5. From the plots, the curve for RCP4.5 is flatter than that for RCP8.5, indicating that the standard deviation is larger for the former. The extreme temperatures are projected to be more clustered around the mean value under RCP4.5, but more spread out with high variability under RCP8.5. Notably, the projection of extreme temperatures under RCP8.5 is higher than that under RCP4.5. Particularly, both RCPs project approximately the same amount of extreme temperatures for the early century.

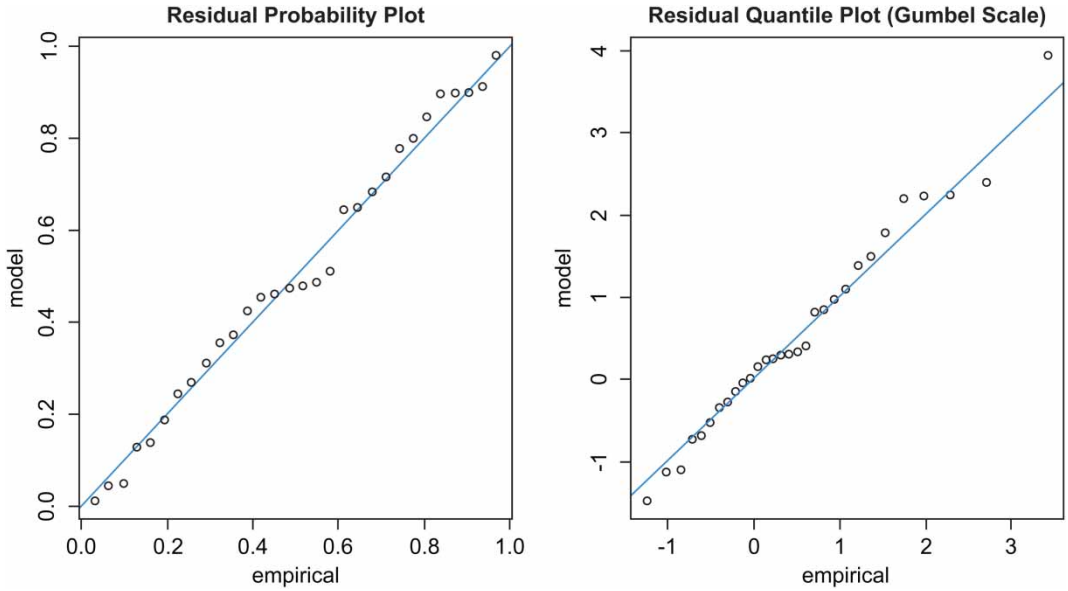

Figure 2 | Quantile and density plots of annual extreme temperatures for station 42.

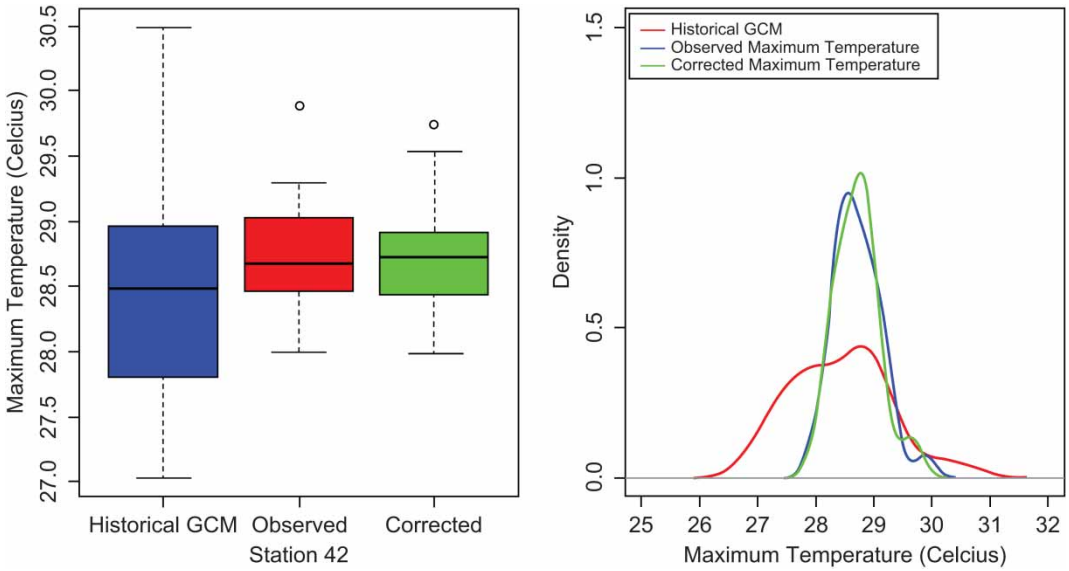

Figure 3 | Historical/estimated, observed, and corrected annual extreme temperatures for station 42.

The projection of extreme temperatures gradually increased toward mid- and late centuries. The projections under RCP8.5 and RCP4.5 are somewhat higher in the late and mid century, respectively. Most of the stations projected extreme temperatures between 30 and 32 °C towards the late century. However, some stations on the western and southern coasts of peninsular Malaysia projected higher extreme temperatures between 33 and 42 °C towards the late century (see also Appendix 5).

3.3. Mortality rate of CVD based on a projection of extreme temperatures

This study focuses on clustering the stations to study the impact of mortality rate because of CVD in different regions (Jolliffe & Philipp 2010). The identification of clusters is based on the similarity of distributions and states (see Appendix 6). This study defines region 1 as Perlis, region 2 as Kedah, region 3 as Pulau Pinang, region 4 as Kelantan and northeast of

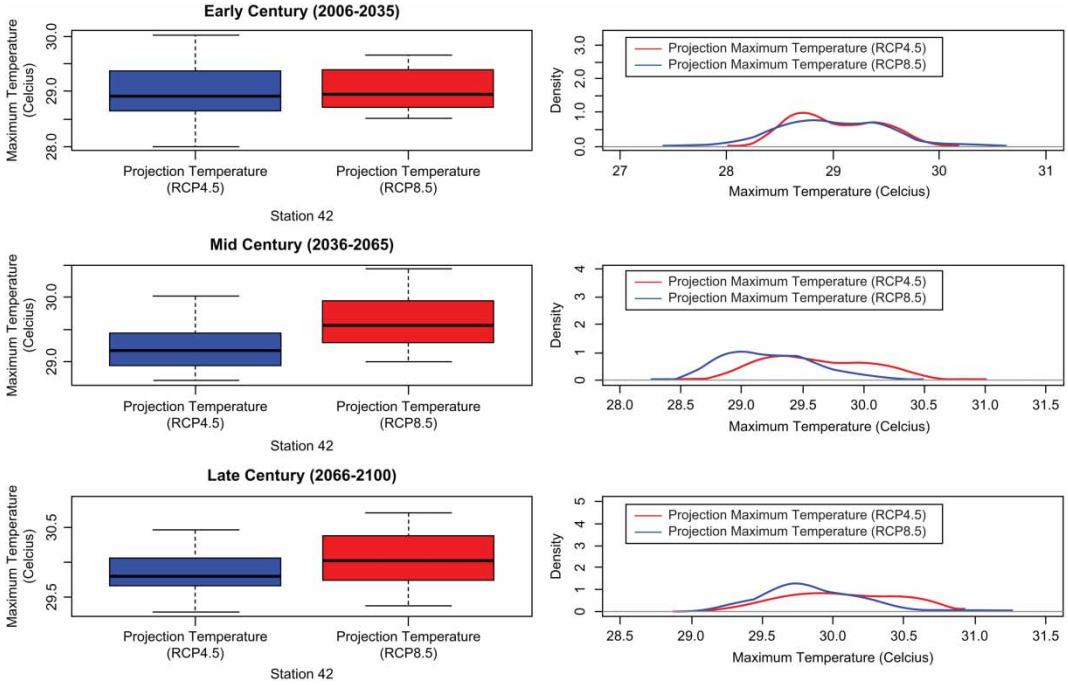

Figure 4 | Projection of future annual extreme temperatures for station 42 under RCP4.5 and RCP8.5 during early, mid-, and late century.

Perak, region 5 as Perak, region 6 as Pahang, region 7 as Terengganu and northeast of Pahang, region 8 as southwest of Perak, region 9 as Kuala Lumpur, Malacca, Negeri Sembilan and Selangor, and region 10 as Johor. Cluster analysis can potentially contribute to the health sector by identifying key targets for these applied initiatives, thereby enabling the allocation of resources in an optimally effective manner and designing efficient adaptation and mitigation strategies in future (Clatworthy *et al.* 2005). The minimum mortality temperature is 28 °C. RR values under RCP8.5 are higher than those under RCP4.5 for all regions. CI describes the inherent uncertainty in this estimate and the range of values within which the true effect lies with reasonable certainty. The effect size is precisely known for small intervals, whereas the uncertainty is greater for larger intervals, i.e., large sample size tends to give more precise estimates of effects, and a small CI corresponds to a small sample size. The projected estimated extreme temperatures are 30–32 °C and 33–42 °C under RCP4.5 and RCP8.5, respectively. Arias *et al.* (2021) stated that there is a high confidence that the temperature change might increase to 1.5 °C and 4 °C toward the late century under RCP4.5 and RCP8.5, respectively. The RR values produced lower uncertainties (high confidence) for extreme temperatures between 30 and 32 °C for regions 1–4, 7–8 under both RCPs, whereas RR values produce lower uncertainties (high confidence) for regions 5–6, 9–10 with extreme temperatures between 33–36 °C and 33–42 °C under RCP4.5 and RCP8.5, respectively. Notice that the RR value for the point estimate of 61 °C produced high uncertainties with very wide interval estimation (extremely low confidence). Thus, the point estimate can be assumed to be an imprecise estimate (Appendix 7). Notably, regions 5–6 and 9–10 project higher extreme temperatures compared to other regions because of the anthropogenic climate change in urban areas caused by human activities, such as burning fossil fuels including coal, oil, and natural gas which leads to severe environmental damage linked to climate change. The high warming rate, particularly in large areas such as Kuala Lumpur, Selangor, and Johor could be enhanced by the urban heat island effect. The short period of data coverage and higher frequency of the El-Niño Southern/Oscillation (ENSO) occurrences in the last few decades may contribute to higher warming rates in some Malaysian stations. Some studies based on shorter data records of the last four or five decades reported higher warming rates (Tangang *et al.* 2007). Furthermore, higher projected extreme temperatures in regions 5 and 6 (≈36 °C) could also be influenced by geographical factors because both regions are situated near the Indian and Pacific oceans in which the inter-annual variability variation in sea surface temperature could influence the large-scale climate variability, such as ENSO and Indian Ocean Dipole (Isa *et al.* 2020).

Figure 5 shows the projection of mortality rate because of CVD in early, mid-, and late century, which is higher under RCP8.5 than RCP4.5 coincides with the projection of extreme temperatures. The median of CVD mortality rate for regions 1 and 4 ranges between 0.0035 and 0.0037 from early to late century under RCP4.5, whereas it ranges between 0.0035 and 0.0042 under RCP8.5. Regions 3 and 7 exhibit the least median value under RCP4.5, which is 0.002; however, the median is

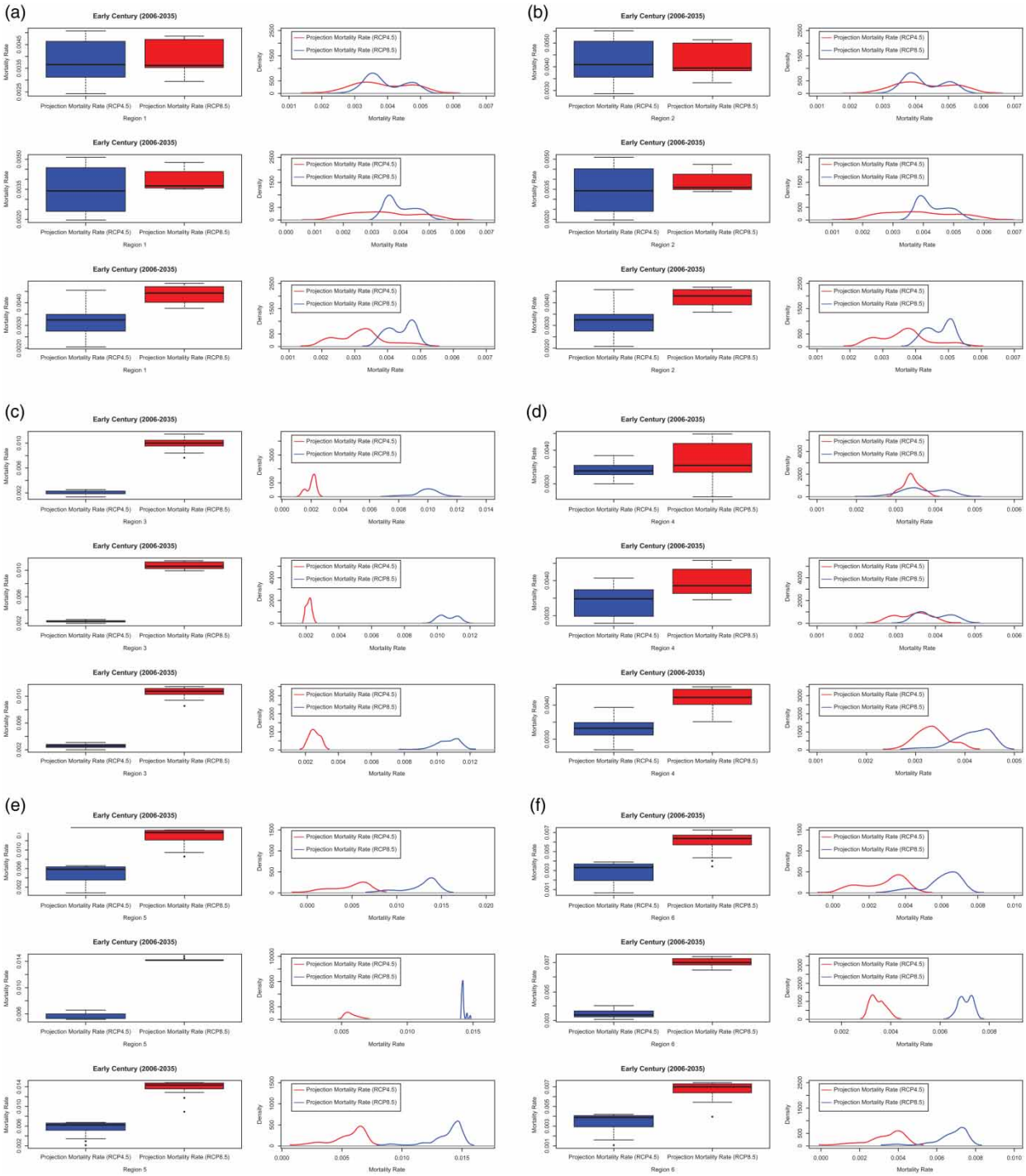

Figure 5 | Projection of CVD mortality rate due based on annual extreme temperatures during early, mid- and late century under RCP4.5 and RCP8.5 for (a) region 1, (b) region 2, (c) region 3, (d) region 4, (e) region 5, (f) region 6, (g) region 7, (h) region 8, (i) region 9, and (j) region 10. (*continued.*).

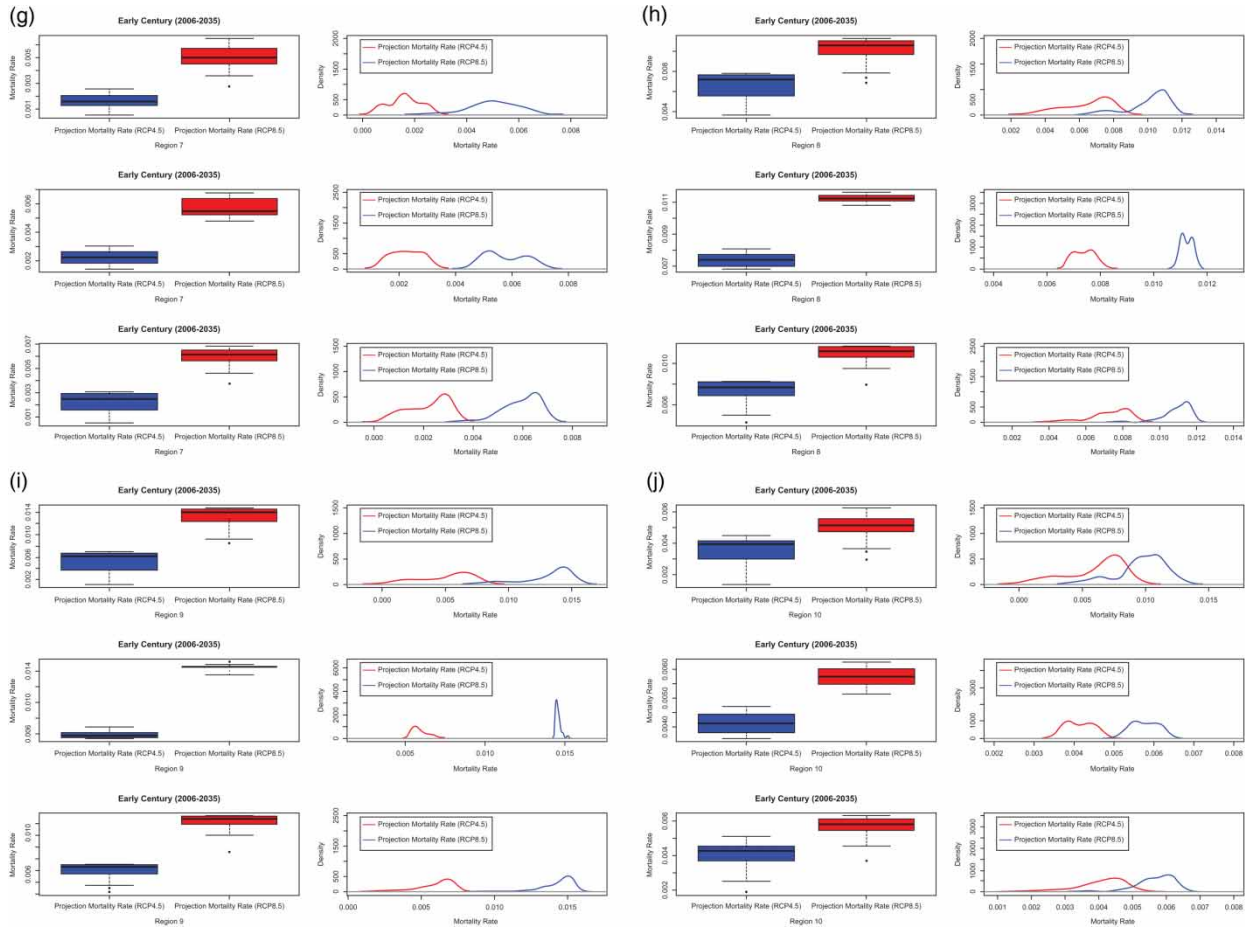

Figure 5 | Continued.

high under RCP8.5 in the range 0.06–0.1. Notably, higher median values of CVD mortality rate for both regions 8 and 9 agree with the higher projected extreme temperatures. The mortality rate for region 8 is 0.06 under RCP4.5 and 0.01 under RCP8.5, whereas it is 0.06 under RCP4.5 and 0.014 under RCP8.5 for region 9. Particularly, the median of CVD mortality rate for region 5 is extraordinarily high under RCP8.5 at 0.014 compared to RCP4.5 at 0.006, corresponding to a higher projected value of extreme temperatures (≈35 °C). Similarly, region 6 also depicted a higher median value of CVD mortality rate under RCP8.5 at 0.007 compared to RCP4.5 at 0.003 with respect to higher projected extreme temperatures. Regions 2 and 10 reported similar values of CVD mortality rate that range approximately between 0.004 and 0.006 under RCP4.5 and RCP8.5, respectively. In terms of the frequency of mortality (per 1,000 population), the highest number of mortalities is expected in regions 5, 8, and 9 with 6 to 14 deaths per year. Although the lower number of mortalities is recorded in region 3 under RCP4.5 (2 deaths per year), it is expected to spike up to 10 deaths per year under RCP8.5. Similarly, regions 6 and 7 expected lower mortality numbers under RCP4.5 (2–3 deaths per year) than in RCP8.5 (6–7 deaths per year). Meanwhile, regions 1, 2, 4, and 10 expected around 3–6 deaths per year. Under some circumstances, the CVD mortality is not as bad under RCP4.5 compared to RCP8.5. Table 2 shows the correlation coefficients between the projections of future annual extreme temperatures and mortality rates because of CVD between 2006 and 2100. The correlations are estimated to identify the significance of the relationship between extreme temperatures and CVD mortality rate in future. For RCP8.5, all regions have *p*-values less than the significance level. Rejecting H_0 at the significance level of 0.05 suggests that the correlation between future extreme temperatures and mortality rate is significant. Correlation values in the range of 0.4–0.6 indicate a moderate positive relationship, and those above 0.7 indicate a strong positive relationship between extreme temperatures and CVD mortality rate. The results are consistent with those of Baaghideh & Mayvaneh (2017), which state that there is a positive and strong correlation between CVD mortality and extreme temperatures higher than 26 °C. Additionally, it is

Table 2 | Correlation coefficient between projections of future annual extreme temperatures and mortality rate because of CVD (2006–2100)

Region	Correlation coefficient value (RCP4.5)	*p*-Value	Region	Correlation coefficient value (RCP8.5)	*p*-Value
1	**0.28**	**0.01**	**1**	**0.47**	**0**
2	**0.24**	**0.02**	**2**	**0.65**	**0**
3	**0.24**	**0.02**	**3**	**0.85**	**0**
4	0.19	0.06	**4**	**0.47**	**0**
5	**0.27**	**0.01**	**5**	**0.43**	**0**
6	0.1	0.34	**6**	**0.9**	**0**
7	**0.38**	**0**	**7**	**0.64**	**0**
8	**0.79**	**0**	**8**	**0.83**	**0**
9	**0.91**	**0**	**9**	**0.94**	**0**
10	**0.31**	**0**	**10**	**− 0.25**	**0.01**

Bold fonts refer to significant correlation coefficients between future extreme temperatures and CVD mortality rate.

observed that there is a weak and moderate but significant (p-value < 0.05) association between extreme temperatures and CVD mortality rate, indicating that both variables vary in the same direction (i.e., they have the same magnitude). Regions 1 and 4–5 have a moderate positive relationship, whereas regions 2–3 and 6–9 have a strong positive relationship. Contrastingly, there is a significant negative correlation in region 10 with correlation values around 0.25 indicating a weak negative relationship between extreme temperatures and CVD mortality rate. The contradiction in the magnitude of relationship might be attributed to a remarkably high extreme temperature (i.e., outlier). As seen, region 10 covers the station 53 that produces an overestimated point estimate of extreme temperatures. The relationship could be misleading because of higher uncertainties. The negative sign is attributed to the large uncertainty around the maximum temperature in region 10. As for RCP4.5, regions 1–3, 5–7, and 10 show a significantly weak positive relationship, whereas regions 8–9 show a significantly strong positive relationship between extreme temperatures and CVD mortality rate. There is no significant correlation coefficient between future extreme temperatures and CVD mortality rate in region 4. However, for RCP8.5 there is a significant positive relationship between annual extreme temperatures and CVD mortality rate in almost every region with correlation coefficients ranging from 0.1 to 0.9, except for region 10.

4. CONCLUSIONS

This study developed BCM-QM_{skewed} by incorporating the skewed distribution and a linear covariate into BCM to better fit the extreme temperatures in peninsular Malaysia. LGNORM and GUM are the most appropriate distributions to model the annual extreme temperatures at stations throughout peninsular Malaysia. LGNORM and GUM are the most suitable models to fit the annual extreme temperatures in the western and eastern parts of peninsular Malaysia, respectively, based on the AIC and BIC diagnostic tests. It can also be inferred that a BCM-QM_{skewed} with time-varying covariate is a good fitted model for annual extreme temperatures at most stations across peninsular Malaysia which suggests that the trend of extreme temperatures has been linearly increasing during 1976–2005. BCM-QM_{skewed} exhibits considerable skills in reducing the biases from the GCM model for all stations. The corrected annual extreme temperatures are comparable to the observed values based on the RMSE, MAE, PBIAS, and PP values. The projection trends for extreme temperatures increase for both RCPs. Higher projection is more pronounced under RCP8.5 with precise estimates ranging between 33 and 42 °C compared to that under RCP4.5 with precise estimates ranging from 30 to 32 °C. The CVD mortality rate falls in the range of 0.002–0.014. Regions 5, 8–9 should be given extra attention because the trend of extreme temperatures has been shown to increase yearly, which may cause higher CVD mortality rates in future, with a median rate that can attain a value of 0.014 (i.e., 14 deaths per year) . Overall, the CVD mortality rate across all regions in peninsular Malaysia is significant, specifically under RCP8.5. However, high CVD mortality rates coincide with high extreme temperatures. The significance of this study rests on the fact that the health sector in Malaysia heavily depends on climatic conditions. Thus, studying future scenarios may provide important information to researchers and local governments, to propose appropriate adaptation measures and increase resilience. Furthermore, appropriate policies and plans can be sanctioned to prepare the public for changes because

of extreme temperatures, particularly, on CVD mortality. Using the accurate predictions of future mortality rates of CVD, the government can play a crucial role by enacting policies that encourage the provision of preventive healthcare services and promotion of a healthy lifestyle. However, the following improvements may be considered in the future. Multi-model ensembles can be used to improve the performance of GCM simulations instead of a single GCM to reduce the uncertainties. The selection of suitable distribution continues to improve with time and hybrid distribution (i.e., a combination of two or more distributions) may be associated with BCM-QM_{skewed}. Furthermore, other causes/factors of CVD and various categories of patients, such as gender, age, and race, could be potentially examined to achieve more meaningful outcomes to assist the respective local authorities, leaders, and policy makers in making action plans and preparing preventive measures. Integrating various climate covariates indifferent to spatio-temporal scale in the BCM-QM_{skewed} model may also be considered for future studies.

ACKNOWLEDGEMENTS

The daily mean temperatures of 58 stations in peninsular Malaysia were obtained from Ir. Dr Wong Chee Loong. We would also like to thank Editage (www.editage.com) for English language editing. This research was funded by the Malaysian Ministry of Higher Education Fundamental Research Grant Scheme (FRGS/1/2018/STG06/UPM/02/5) grant number 5540130.

DATA AVAILABILITY STATEMENT

All relevant data are available from http://ghdx.healthdata.org/gbd-results-tool.

CONFLICT OF INTEREST

The authors declare there is no conflict.

REFERENCES

Abatzoglou, J. T. & Brown, T. J. 2012 A comparison of statistical downscaling methods suited for wildfire applications. *International Journal of Climatology* **32** (5), 772–780.

Adeyeri, O., Laux, P., Lawin, A. & Oyekan, K. 2020 Multiple bias-correction of dynamically downscaled cmip5 climate models temperature projection: a case study of the transboundary Komadugu-Yobe river basin, Lake Chad region, West Africa. *SN Applied Sciences* **2** (7), 1–18.

Amin, N. A. M., Ismail, M. S. & Hamid, H. A. 2018 Modelling extreme temperatures in perlis using block maxima method. In *AIP Conference Proceedings*, 2013. AIP Publishing LLC, pp. 020010.

Amirabadizadeh, M., Ghazali, A. H., Huang, Y. F. & Wayayok, A. 2016 Downscaling daily precipitation and temperatures over the Langat river basin in Malaysia: a comparison of two statistical downscaling approaches. *International Journal of Water Resources and Environmental Engineering* **8** (10), 120–136.

An, D., Du, Y., Berndtsson, R., Niu, Z., Zhang, L. & Yuan, F. 2020 Evidence of climate shift for temperature and precipitation extremes across Gansu province in China. *Theoretical and Applied Climatology* **139** (3), 1137–1149.

Arias, P., Bellouin, N., Coppola, E., Jones, R., Krinner, G., Marotzke, J., Naik, V., Palmer, M., Plattner, G.-K., Rogelj, J., Rojas, M., Sillmann, J., Storelvmo, T., Thorne, P., Trewin, B., Achutarao, K., Adhikary, B., Allan, R., Armour, K., Bala, G., Barimalala, R., Berger, S., Canadell, J. G., Cassou, C., Cherchi, A., Collins, W. D., Collins, W. J., Connors, S., Corti, S., Cruz, F., Dentener, F. J., Dereczynski, C., Di Luca, A., Diongue Niang, A., Doblas-Reyes, P., Dosio, A., Douville, H., Engelbrecht, F., Eyring, V., Fischer, E. M., Forster, P., Fox-Kemper, B., Fuglestvedt, J., Fyfe, J., Gillett, N., Goldfarb, L., Gorodetskaya, I., Gutierrez, J. M., Hamdi, R., Hawkins, E., Hewitt, H., Hope, P., Islam, A. S., Jones, C., Kaufmann, D., Kopp, R., Kosaka, Y., Kossin, J., Krakovska, S., Li, J., Lee, J.-Y., Masson-Delmotte, V., Mauritsen, T., Maycock, T., Meinshausen, M., Min, S., Ngo Duc, T., Otto, F., Pinto, I., Pirani, A., Raghavan, K., Ranasighe, R., Ruane, A., Ruiz, L., Sallée, J.-B., Samset, B. H., Sathyendranath, S., Monteiro, P. S., Seneviratne, S. I., Sörensson, A. A., Szopa, S., Takayabu, I., Treguier, A.-M., van den Hurk, B., Vautard, R., Von Schuckmann, K., Zaehle, S., Zhang, X. & Zickfeld, K. 2021 Climate change 2021: The physical science basis. Contribution of Working Group 14 I to the Sixth Assessment Report of the Intergovernmental Panel on Climate Change; Technical Summary.

Baaghideh, M. & Mayvaneh, F. 2017 Climate change and simulation of cardiovascular disease mortality: a case study of Mashhad, Iran. *Iranian Journal of Public Health* **46**, 396.

Barrow, E. & Hulme, M. 1996 Changing probabilities of daily temperature extremes in the UK related to future global warming and changes in climate variability. *Climate Research* **6** (1), 21–31.

Bettolli, M. L., Solman, S. A., Da Rocha, R. P., Llopart, M., Gutierrez, J. M., Fernández, J., Olmo, M. E., Lavin-Gullon, A., Chou, S. C., Rodrigues, C. D., Coppola, E., Huarte, R. B., Barreiro, M., Blázquez, J., Doyle, M., Feijoó, M., Huth, R., Machado, L. & Cuadra, S. V. 2021 The CORDEX Flagship Pilot Study in southeastern South America: a comparative study of statistical and dynamical downscaling models in simulating daily extreme precipitation events. *Climate Dynamics* **56** (5), 1589–1608.

Cannon, A. J., Sobie, S. R. & Murdock, T. Q. 2015 Bias correction of GCM precipitation by quantile mapping: how well do methods preserve changes in quantiles and extremes? *Journal of Climate* **28** (17), 6938–6959.

Clatworthy, J., Buick, D., Hankins, M., Weinman, J. & Horne, R. 2005 The use and reporting of cluster analysis in health psychology: a review. *British Journal of Health Psychology* **10** (3), 329–358.

Coles, S., Bawa, J., Trenner, L. & Dorazio, P. 2001 *An Introduction to Statistical Modeling of Extreme Values*, Vol. 208. Springer, London, p. 208.

Conlon, K. C., Kintziger, K. W., Jagger, M., Stefanova, L., Uejio, C. K. & Konrad, C. 2016 Working with climate projections to estimate disease burden: perspectives from public health. *International Journal of Environmental Research and Public Health* **13** (8), 804.

Crimmins, A., Bell, J., Fann, N. & Hawkins, M. 2016 The impacts of climate change on human health in the United States. In *A Scientific Assessment 2016*. US Global Change Research Program, Washington, DC.

De' Donato, F. K., Leone, M., Scortichini, M., De Sario, M., Katsouyanni, K., Lanki, T., Basagaña, X., Ballester, F., Åström, C., Paldy, A., Pascal, M., Gasparrini, A., Menne, B. & Michelozzi, P. 2015 Changes in the effect of heat on mortality in the last 20 years in nine European cities. results from the phase project. *International Journal of Environmental Research and Public Health* **12** (12), 15567–15583.

DOSM 2017 Statistics causes of deaths, Malaysia, 2017.

DOSM 2018 Statistics causes of deaths, Malaysia, 2018.

DOSM 2019 Statistics causes of deaths, Malaysia, 2019.

DOSM 2020 Statistics causes of deaths, Malaysia, 2020.

Enayati, M., Bozorg-Haddad, O., Bazrafshan, J., Hejabi, S. & Chu, X. 2021 Bias correction capabilities of quantile mapping methods for rainfall and temperature variables. *Journal of Water and Climate Change* **12** (2), 401–419.

Etemadi, H., Samadi, S. & Sharifikia, M. 2014 Uncertainty analysis of statistical downscaling models using general circulation model over an international wetland. *Climate Dynamics* **42**, 2899–2920.

Fang, G., Yang, J., Chen, Y. & Zammit, C. 2015 Comparing bias correction methods in downscaling meteorological variables for a hydrologic impact study in an arid area in China. *Hydrology and Earth System Sciences* **19**, 2547–2559.

Folland, C., Miller, C., Bader, D., Crowe, M., Jones, P., Plummer, N., Richman, M., Parker, D., Rogers, J. & Scholefield, P. 1999 Workshop on indices and indicators for climate extremes, Asheville, NC, USA, 3–6 June 1997 breakout group C: temperature indices for climate extremes. *Climatic Change* **42** (1), 31–43.

Gaitán, E., Monjo, R., Pórtoles, J. & Pino-Otín, M. R. 2019 Projection of temperatures and heat and cold waves for Aragón (Spain) using a two-step statistical downscaling of CMIP5 model outputs. *Science of the Total Environment* **650**, 2778–2795.

Gasparrini, A. 2013 Distributed lag linear and non-linear models for time series data, Document is available at R project.

Grillakis, M. G., Koutroulis, A. G. & Tsanis, I. K. 2013 Multisegment statistical bias correction of daily GCM precipitation output. *Journal of Geophysical Research: Atmospheres* **118** (8), 3150–3162.

Gu, S., Zhang, L., Sun, S., Wang, X., Lu, B., Han, H., Yang, J. & Wang, A. 2020 Projections of temperature-related cause-specific mortality under climate change scenarios in a coastal city of China. *Environment International* **143**, 105889.

Hajat, S., Kovats, R. S., Atkinson, R. W. & Haines, A. 2002 Impact of hot temperatures on death in London: a time series approach. *Journal of Epidemiology and Community Health* **56** (5), 367–372.

Hajat, S., Vardoulakis, S., Heaviside, C. & Eggen, B. 2014 Climate change effects on human health: projections of temperature-related mortality for the UK during the 2020s, 2050 and 2080s. *Journal of Epidemiology & Community Health* **68** (7), 641–648.

Hasan, H., Salam, N. & Kassim, S. 2013 Modeling annual extreme temperatures using generalized extreme value distribution: a case study in Malaysia. In: *AIP Conference Proceedings*, Vol. 1522 (A. Ishak, I. Hashim, E. S. Ismail & R. Nazar, eds.). American Institute of Physics, College Park, MD, pp. 1195–1203.

Hasan, H., Salleh, N. H. M. & Kassim, S. 2014 Stationary and non-stationary extreme value modeling of extreme temperatures in Malaysia. In: *AIP Conference Proceedings*, Vol. 1613 (M. Shitan, L.S. Lee & Z. K. Eshkuvatov, eds.). American Institute of Physics, College Park, MD, pp. 355–367.

Hempel, S., Frieler, K., Warszawski, L., Schewe, J. & Piontek, F. 2013 A trend-preserving bias correction – the ISI-MIP approach. *Earth System Dynamics* **4** (2), 219–236.

Higgins, J. P., Thomas, J., Chandler, J., Cumpston, M., Li, T., Page, M. J. & Welch, V. A. 2019 *Cochrane Handbook for Systematic Reviews of Interventions*. John Wiley & Sons, Chichester, UK.

Holthuijzen, M. F., Beckage, B., Clemins, P. J., Higdon, D. & Winter, J. M. 2021 Constructing high-resolution, bias-corrected climate products: a comparison of methods. *Journal of Applied Meteorology and Climatology* **60** (4), 455–475.

Hong, J., Agustin, W., Yoon, S. & Park, J. S. 2022 Changes of extreme precipitation in the Philippines, projected from the CMIP6 multi-model ensemble. *Weather and Climate Extremes* **37**, 100480.

Horton, E., Folland, C. & Parker, D. 2001 The changing incidence of extremes in world- wide and central England temperatures to the end of the twentieth century. *Climatic Change* **50** (3), 267–295.

Huang, C., Barnett, A. G., Wang, X. & Tong, S. 2012 Effects of extreme temperatures on years of life lost for cardiovascular deaths: a time series study in Brisbane, Australia. *Circulation: Cardiovascular Quality and Outcomes* **5** (5), 609–614.

Huang, J., Zeng, Q., Pan, X., Guo, X. & Li, G. 2019 Projections of the effects of global warming on the disease burden of ischemic heart disease in the elderly in Tianjin, China. *BMC Public Health* **19** (1), 1–9.

Huynen, M. M., Martens, P., Schram, D., Weijenberg, M. P. & Kunst, A. E. 2001 The impact of heat waves and cold spells on mortality rates in the Dutch population. *Environmental Health Perspectives* **109** (5), 463–470.

Isa, N. S., Akhir, M. F., Kok, P. H., Daud, N. R., Khalil, I. & Roseli, N. H. 2020 Spatial and temporal variability of sea surface temperature during El-Niño Southern Oscillation and Indian Ocean Dipole in the strait of malacca and andaman Sea. *Regional Studies in Marine Science* **39**, 101402.

Jackson, J. E., Yost, M. G., Karr, C., Fitzpatrick, C., Lamb, B. K., Chung, S. H., Chen, J., Avise, J., Rosenblatt, R. A. & Fenske, R. A. 2010 Public health impacts of climate change in Washington state: projected mortality risks due to heat events and air pollution. *Climatic Change* **102** (1), 159–186.

Jolliffe, I. T. & Philipp, A. 2010 Some recent developments in cluster analysis. *Physics and Chemistry of the Earth A/B/C* **35** (9), 309–315.

Jones, P. D., Horton, E. B., Folland, C. K., Hulme, M., Parker, D. E. & Basnett, T. A. 1999 The use of indices to identify changes in climatic extremes. *Climatic Change* **42** (1), 131–149.

Jose, D. M., Vincent, A. M. & Dwarakish, G. S. 2022 Improving multiple model ensemble predictions of daily precipitation and temperature through machine learning techniques. *Scientific Reports* **12** (1), 1–25.

Kharin, V. V. & Zwiers, F. W. 2005 Estimating extremes in transient climate change simulations. *Journal of Climate* **18** (8), 1156–1173.

Kouis, P., Kakkoura, M., Ziogas, K., Paschalidou, A. K. & Papatheodorou, S. I. 2019 The effect of ambient air temperature on cardiovascular and respiratory mortality in Thessaloniki, Greece. *Science of The Total Environment* **647**, 1351–1358.

Kynast-Wolf, G., Preuss, M., Sie, A., Kouyate, B. & Becher, H. 2010 Seasonal patterns of cardiovascular disease mortality of adults in Burkina Faso, West Africa. *Tropical Medicine and International Health* **15**, 1082–1089.

Lafon, T., Dadson, S., Buys, G. & Prudhomme, C. 2013 Bias correction of daily precipitation simulated by a regional climate model: a comparison of methods. *International Journal of Climatology* **33** (6), 1367–1381.

Lange, S. 2019 Trend-preserving bias adjustment and statistical downscaling with ISIMIP3BASD (v1. 0). *Geoscientific Model Development* **12** (7), 3055–3070.

Li, T., Horton, R. M. & Kinney, P. 2013 Future projections of seasonal patterns in temperature-related deaths for Manhattan. *Nature Climate Change* **3**, 717–721.

Li, G., Guo, Q., Liu, Y., Li, Y. & Pan, X. 2018 Projected temperature-related years of life lost from stroke due to global warming in a temperate climate city, Asia: disease burden caused by future climate change. *Stroke* **49** (4), 828–834.

Liu, T., Ren, Z., Zhang, Y., Feng, B., Lin, H., Xiao, J., Zeng, W., Li, X., Li, Z., Rutherford, S., Xu, Y., Lin, S., Nasca, P. C., Du, Y., Wang, J., Huang, C., Jia, P. & Ma, W. 2019 Modification effects of population expansion, ageing, and adaptation on heat-related mortality risks under different climate change scenarios in Guangzhou, China. *International Journal of Environmental Research and Public Health* **16** (3), 376.

Mamalakis, A., Langousis, A., Deidda, R. & Marrocu, M. 2017 A parametric approach for simultaneous bias correction and high-resolution downscaling of climate model rainfall. *Water Resources Research* **53** (3), 2149–2170.

Maurer, E. P. & Hidalgo, H. G. 2008 Utility of daily vs. monthly large-scale climate data: an intercomparison of two statistical downscaling methods. *Hydrology and Earth System Sciences* **12** (2), 551–563.

McGeehin, M. A. & Mirabelli, M. 2001 The potential impacts of climate variability and change on temperature-related morbidity and mortality in the United States. *Environmental Health Perspectives* **109** (suppl 2), 185–189.

Moghadamnia, M. T., Ardalan, A., Mesdaghinia, A., Keshtkar, A., Naddafi, K. & Yekaninejad, M. S. 2017 Ambient temperature and cardiovascular mortality: a systematic review and meta-analysis. *Peer J* **5**, e3574.

Murphy, J. 1999 An evaluation of statistical and dynamical techniques for downscaling local climate. *Journal of Climate* **12** (8), 2256–2284.

Ng, J. L., Chan, K. H., Noh, N. M., Razman, R., Surol, S., Lee, J. C. & Al-Mansob, R. A. 2022 Statistical modelling of extreme temperatures in peninsular Malaysia. In IOP Conference Series: Earth and Environmental Science. 1022(1), 012072, IOP Publishing.

Ngai, S. T., Juneng, L., Tangang, F., Chung, J. X., Supari, S., Salimun, E., Cruz, F., Ngo-Duc, T., Phan-Van, T., Santisirisomboon, J. & Gunawan, D. 2022 Projected mean and extreme precipitation based on bias-corrected simulation outputs of CORDEX Southeast Asia. *Weather and Climate Extremes* **37**, 100484.

Noor, M., Ismail, T., Chung, E.-S., Shahid, S. & Sung, J. H. 2018 Uncertainty in rainfall intensity duration frequency curves of peninsular Malaysia under changing climate scenarios. *Water* **10** (12), 1750.

Olsson, T., Jakkila, J., Veijalainen, N., Backman, L., Kaurola, J. & Vehviläinen, B. 2015 Impacts of climate change on temperature, precipitation and hydrology in Finland – studies using bias corrected Regional Climate Model data. *Hydrology and Earth System Sciences* **19** (7), 3217–3238.

Paravantis, J., Santamouris, M., Cartalis, C., Efthymiou, C. & Kontoulis, N. 2017 Mortality associated with high ambient temperatures, heatwaves, and the urban heat island in Athens, Greece. *Sustainability* **9** (4), 606.

Pastén-Zapata, E., Jones, J. M., Moggridge, H. & Widmann, M. 2020 Evaluation of the performance of Euro-CORDEX regional climate models for assessing hydrological climate change impacts in Great Britain: a comparison of different spatial resolutions and quantile mapping bias correction methods. *Journal of Hydrology* **584**, 124653.

Patel, L., Conlon, K. C., Sorensen, C., McEachin, S., Nadeau, K., Kakkad, K. & Kizer, K. W. 2022 Climate change and extreme heat events: how health systems should prepare. *NEJM Catalyst Innovations in Care Delivery* **3** (7), CAT-21.

Piani, C., Weedon, G., Best, M., Gomes, S., Viterbo, P., Hagemann, S. & Haerter, J. 2010 Statistical bias correction of global simulated daily precipitation and temperature for the application of hydrological models. *Journal of Hydrology* **395** (3–4), 199–215.

Putra, I. D. G. A., Rosid, M. S., Sopaheluwakan, A. & Sianturi, Y. C. U. 2020 The CMIP5 projection of extreme climate indices in Indonesia using simple quantile mapping method. In: *AIP Conference Proceedings*. Vol. 2223. AIP Publishing LLC, p. 050008.

Raggad, B. 2018 Stationary and non-stationary extreme value approaches for modelling extreme temperatures: the case of Riyadh city, Saudi Arabia. *Environmental Modeling & Assessment* **23** (1), 99–116.

Räisänen, J. & Räty, O. 2013 Projections of daily mean temperature variability in the future: cross-validation tests with ENSEMBLES regional climate simulations. *Climate Dynamics* **41** (5), 1553–1568.

Ringard, J., Seyler, F. & Linguet, L. 2017 A quantile mapping bias correction method based on hydroclimatic classification of the Guiana Shield. *Sensors* **17** (6), 1413.

Roth, G. A. 2018 Global Burden of Disease Collaborative Network. Global Burden of Disease Study 2017 (GBD 2017) Results. Seattle, United States: Institute for Health Metrics and Evaluation (IHME), 2018. *The Lancet* **392**, 1736–1788.

Salleh, N. H. M. & Hasan, H. 2018 Generalized pareto distribution for extreme temperatures in peninsular Malaysia. *Science International (Lahore)* **30**, 63–67.

Seimela, A. M. 2021 *Modelling Temperature Extremes in the Limpopo Province of South Africa Using Extreme Value Theory*. PhD Thesis.

Semenov, M. A. 2008 Simulation of extreme weather events by a stochastic weather generator. *Climate Research* **35** (3), 203–212.

Sennikovs, J., Bethers, U., 2009 Statistical downscaling method of regional climate model results for hydrological modelling. In *18th World IMACS Congress and MODSIM09 International Congress on Modelling and Simulation*. Anderssen, R. S., Braddock, R. D. & Newham, L. T. H. Citeseer, pp. 3962–3968.

Shaaban, A. J., Amin, M., Chen, Z. & Ohara, N. 2011 Regional modeling of climate change impact on peninsular Malaysia water resources. *Journal of Hydrologic Engineering* **16** (12), 1040–1049.

Shrestha, R. R., Schnorbus, M. A., Werner, A. T. & Zwiers, F. W. 2014 Evaluating hydro-climatic change signals from statistically and dynamically downscaled GCMs and hydrologic models. *Journal of Hydrometeorology* **15** (2), 844–860.

Smid, M. & Costa, A. C. 2018 Climate projections and downscaling techniques: a discussion for impact studies in urban systems. *International Journal of Urban Sciences* **22** (3), 277–307.

Sridhar, S., Fazelpour, M., Gill, A. S. & Summers, J. D. 2016 Accuracy and precision analysis of the graph complexity connectivity method. *Procedia CIRP* **44**, 163–168.

Stocker, T. 2014 *Climate Change 2013: the Physical Science Basis: Working Group I Contribution to the Fifth Assessment Report of the Intergovernmental Panel on Climate Change*. Cambridge University Press, Cambridge, UK.

Suhaila, J. & Yusop, Z. 2018 Trend analysis and change point detection of annual and seasonal temperature series in peninsular Malaysia. *Meteorol. Atmospheric Phys.* **130** (4), 1–17.

Suparta, W. & Yatim, A. N. M. 2017 An analysis of heat wave trends using heat index in east Malaysia. *Journal of Physics: Conference Series* **852**, 012005.

Suparta, W. & Yatim, A. N. M. 2019 Characterization of heat waves: a case study for peninsular Malaysia. *Geographia Technica* **14** (1), 146–155.

Supian, N. M. & Hasan, H. 2021 Selecting the probability distribution of annual maximum temperature in Malaysia. In *ITM Web of Conferences*, Vol. 36. EDP Sciences.

Tadese, M. T., Kumar, L. & Koech, R. 2020 Climate change projections in the awash river basin of Ethiopia using global and regional climate models. *International Journal of Climatology* **40** (8), 3649–3666.

Tangang, F. T., Juneng, L. & Ahmad, S. 2007 Trend and interannual variability of temperature in Malaysia: 1961–2002. *Theoretical and Applied Climatology* **89** (3), 127–141.

Tangang, F., Chung, J. X., Juneng, L., Supari, S., Ngai, S. T., Jamaluddin, A. F., Faisal, M. S., Cruz, F., Narisma, G. T., Santisirisomboon, J., Ngo-Duc, T., Phan, V. T., Singhruck, P., Gunawan, D., Aldrian, E., Sopaheluwakan, A., Nikulin, G., Remedio, A. R. C., Sein, D. V., Hein-Griggs, D. & Mcgregor, J. L. 2020 Projected future changes in rainfall in Southeast Asia based on CORDEX–SEA multi-model simulations. *Climate Dynamics* **55** (2), 1247–1267.

Teutschbein, C. & Seibert, J. 2012 Bias correction of regional climate model simulations for hydrological climate-change impact studies: review and evaluation of different methods. *Journal of Hydrology* **456**, 12–29.

Underwood, F. 2013 Describing seasonal variability in the distribution of daily effective temperatures for 1985–2009 compared to 1904–1984 for de Bilt, Holland. *Meteorological Applications* **20** (4), 394–404.

Vaidyanathan, A., Malilay, J., Schramm, P. & Saha, S. 2020 Heat-related deaths-United States, 2004–2018. *Morbidity and Mortality Weekly Report* **69** (24), 729.

Vicedo-Cabrera, A. M., Sera, F. & Gasparrini, A. 2019 Hands-on tutorial on a modeling framework for projections of climate change impacts on health. *Epidemiology (Cambridge, Mass.)* **30** (3), 321.

Wang, J., Moore, J. C., Zhao, L., Yue, C. & Di, Z. 2022 Regional dynamical and statistical downscaling temperature, humidity and windspeed for the Beijing region under stratospheric aerosol injection geoengineering. *Earth System Dynamics Discussions* 1–33.

Wilby, R. L., Hay, L. E., Gutowski, W. J., Arritt, R. W., Takle, E. S., Pan, Z., Leavesley, G. H. & Clark, M. P. 2000 Hydrological responses to dynamically and statistically downscaled climate model output. *Geophysical Research Letters* **27** (8), 1199–1202.

Williams, C., Allan, R. & Kniveton, D. 2012 Diagnosing atmosphere–land feedbacks in CMIP5 climate models. *Environmental Research Letters* **7** (4), 044003.

Wilson, M. K. 2016 *Modelling Extreme Temperatures Behaviour in Upper East Region, Ghana*. PhD Thesis.

Wong, C., Venneker, R., Jamil, A. & Uhlenbrook, S. 2011 Development of a gridded daily hydrometeorological data set for peninsular Malaysia. *Hydrological Processes* **25** (7), 1009–1020.

Wood, A. W., Leung, L. R., Sridhar, V. & Lettenmaier, D. 2004 Hydrologic implications of dynamical and statistical approaches to downscaling climate model outputs. *Climatic Change* **62** (1), 189–216.

World Health Organization 2019 *Quantitative Risk Assessment of the Effects of Climate Change on Selected Causes of Death, 2030 and 2050s*. World Health Organization, Geneva, Switzerland.

Zhan, W., He, X., Sheffield, J. & Wood, E. F. 2020 Projected seasonal changes in large-scale global precipitation and temperature extremes based on the CMIP5 ensemble. *Journal of Climate* **33** (13), 5651–5671.

First received 7 June 2022; accepted in revised form 27 September 2022. Available online 6 October 2022